# Balancing power density based quantum yield characterization of upconverting nanoparticles for arbitrary excitation intensities.

Liu, Haichun; Xu, Can; Lindgren, David; Xie, Haiyan; Thomas, Diana; Gundlach, Carsten; Andersson-Engels, Stefan

*Published in:*
Nanoscale

*DOI:*
10.1039/c3nr00469d

2013

# Balancing power density based quantum yield characterization of upconverting nanoparticles for arbitrary excitation intensities

**Haichun Liu,*[a] Can T. Xu,[a] David Lindgren,[b] Haiyan Xie,[a] Diana Thomas,[c] Carsten Gundlach,[c‡] and Stefan Andersson-Engels[a]**

***Received 26th January 2013, Accepted 15th March 2013***
***First published on the web 20th March 2013***
**DOI: 10.1039/C3NR00469D**

Upconverting nanoparticles (UCNPs) have recently shown great potentials as contrast agents in biological applications. In developing different UCNPs, the characterization on their quantum yield (QY) is a crucial issue, as the typically drastic decrease in QY for low excitation power densities can either impose a severe limitation or provide an opportunity in many applications. The power density dependence of the QY is governed by the competition between the energy transfer upconversion (ETU) rate and the linear decay rate in the depopulation of the intermediate state of the involved activator in the upconversion process. Here we show that the QYs of $Yb^{3+}$ sensitized two-photon upconversion emissions can be well characterized by the balancing power density, at which the ETU rate and the linear decay rate have equal contributions, and its corresponding QY. The results in this paper provide a method to fully describe the QY of upconverting nanoparticles for arbitrary excitation power densities, and is a fast and simple approach for assessing the applicability of UCNPs from the perspective of energy conversion.

## 1 Introduction

Upconverting nanoparticles (UCNPs) doped with rare-earth ions have been rapidly developing during the last decade,[1–5] and their unique properties together with very promising results suggest that they have the potential to become a major class of contrast agents in the field of biophotonics.[6–10] This is mainly due to their ability to convert low energy excitation photons into emission photons with higher energy,[11] even under broadband excitation.[12] This upconversion (UC) ability provides advantages including autofluorescence rejection,[13] better light penetration and improved spatial image resolution.[7,14,15] So far, UCNPs have been successfully used in diverse biological applications such as photodynamic therapy (PDT),[8] microscopy,[9,10] bioanalytical assays,[16,17] diffuse optical imaging,[7,15,18,19] and multimodality imaging.[20] Although UCNPs have many beneficial properties for biological applications, a major challenge of their use is the power density dependent and relatively low QYs under the low excitation intensities required for these applications.[21] It has been reported that UCNPs could have QYs on the order of a few percent at high excitation intensities where the UCNPs are saturated,[14] while the QYs could decline by many orders of magnitude when they are used under low excitation intensities.[14] Obviously, such power density dependent QYs need to be properly evaluated in order to assess the applicability of UCNPs in specific biomedical areas. In spite of the interest, this crucial issue has not been addressed in any satisfactory manner, neither theoretically nor experimentally.[22] Up to date, the reports on the QYs of UCNPs are surprisingly scarce in the literature,[14,23–26] and even in the few publications available, the QY data are usually provided at a specific excitation intensity, ignoring their power density dependency.[23–26] Although full QY information can be obtained by extensive measurements at all excitation intensities, obviously this approach is not ideal because of the accompanying burden of such measurements. In addition, large errors would be also introduced in the measurements at high excitation intensities due to saturation effects of the optical equipments, such as the attenuator and the power meter typically needed for such measurements. This will ruin the accuracy of the QY data. Hence, a better understanding of the power density dependency of the QY for a particular design of UCNPs and thus characterizing this in a convenient way is highly desirable, and will be of major importance for the future development and applications of UCNPs in general. This is addressed in this paper.

The power density dependence of the QY is governed by the competition between the two major relaxation mechanisms involved at the intermediate energy state in the UC process, *i.e.,* the energy transfer upconversion (ETU) and the linear decay.[27,28] In this paper, the dependence of the QY of $Yb^{3+}$

[a] *Division of Atomic Physics, Department of Physics, Lund University, P.O. Box 118, S-221 00 Lund, Sweden. Fax: +46 46 222 4250; Tel: +46 46 222 7471; E-mail: haichun.liu@fysik.lth.se*
[b] *Division of Solid State Physics, Department of Physics, Lund University, P.O. Box 118, S-221 00 Lund, Sweden.*
[c] *MAX IV Laboratory, Lund University, P.O. Box 118, S-221 00 Lund, Sweden.*
‡ Present address:Department of Physics, Technical University of Denmark, 2800 Kgs. Lyngby, Denmark.

sensitized two-photon UC emission on the excitation intensity is modeled using steady-state rate equation analysis, with the activator described by a quasi-three-level structure (including the ground, intermediate and emitting states). It is found that the power density dependent QY can be well characterized by the balancing power density, at which the ETU rate and the linear decay rate equally contribute to the depopulation of the intermediate state of the activator, and the QY at this balancing point. This is experimentally exemplified using near infrared (NIR) emitting $Yb^{3+}/Tm^{3+}$ codoped $NaYF_4$ UCNPs. Thus, the determination of the balancing power density and its corresponding QY is suggested as a fast approach for characterizing the power density dependent QYs of UCNPs, for the sake of assessing the applicability of UCNPs in biological applications from the perspective of energy conversion.

## 2 Experimental

### 2.1 Synthesis of the UCNPs

All the chemicals were purchased from Sigma-Aldrich and used without further purification. The core nanoparticles were synthesized through a recently reported approach.[29] In a typical synthesis procedure, 0.75 mmol $YCl_3$, 0.25 mmol $YbCl_3$ and 0.003 mmol $TmCl_3$ were mixed with 6 mL oleic acid and 17 mL octadecene in a 250 mL flask and heated to 160 °C for 30 min to form a clear solution. After cooling down to room temperature, 10 mL of a methanol solution containing 4 mmol $NH_4F$ (0.1482 g) and 2.5 mmol NaOH (0.1 g) was added, followed by a stirring of the mixture for 30 min at 50 °C. By slowly heating the solution, the methanol was removed and the resulting solution was heated to 300 °C for 1.5 h under argon atmosphere, and then cooled to room temperature. The nanoparticles were precipitated with ethanol and washed with ethanol/water mixture for three times, and then collected after centrifugation and redispersed in a nonpolar solvent. The core–shell nanoparticles were produced by slightly modifying the above procedure through incorporating the prepared core nanoparticles as the seeds in the synthesis.[30] 1 mmol $YCl_3$ was solely used to provide rare-earth ions for the coating layer. Due to the presence of the capping ligand, both the core and core–shell nanoparticles could be well dispersed in commonly used nonpolar solvents, such as hexane, cyclohexane, chloroform, and toluene, and are colloidally stable for months without visible agglomeration.

### 2.2 Characterization of the UCNPs

TEM images were recorded on a JEOL model 3000F microscope. XRD measurements of UCNP hexane suspensions were performed at the crystallography beamline I711 at the synchrotron facility MAXlab, Lund, Sweden.[31] A wavelength of 1.01 Å was employed in the measurements. The samples were placed in glass capillaries with a diameter of 0.5 mm which rotated during data acquisition. The data were recorded by a Titan CCD camera placed 70 mm from the sample. For the PL measurements, a Thorlabs L975P1WJ laser diode at 975 nm was utilized as the excitation source driven by a Thorlabs benchtop LD current controller LDC220C, with the temperature stabilized at 25 °C. The downconversion infrared luminescence was collected by a 20× objective lens with an NA of 0.45 and further directed through two pieces of Spectrogon LP-1000 nm long-pass filters in order to minimize any influence of reflected laser light. The luminescence light was then diffracted in a monochromator by a 150 gr/mm grating blazed at 1200 nm and finally detected by a liquid $N_2$-cooled NIR HgCdTe camera. The UC luminescence spectra were measured on a sensitive spectrofluorometer setup using the same 975 nm laser diode as the excitation source.[14] The emissions were recorded using a grating spectrometer Ocean Optics QE65000 with a slit width of 50 $\mu$m. The excitation power was measured using an Ophir Nova II laser power meter equipped with a photodiode sensor (PD300), while the spot size of the excitation beam was measured using a Hamamatsu ORCA-ER C4742-80 camera. For QY measurements, the system utilized standard fluorophores as a reference, calibrated using the integrating-sphere based Hamamatsu C9920 QY measurement system. The principle of the QY measurement was decribed in detail in our previously published work.[14] All optical measurements were carried out at room temperature.

## 3 Results and discussion

### 3.1 Quantitative analysis using rate equations

The mechanism of $Yb^{3+}$ sensitized two-photon UC emission is simplified and schematically depicted in Fig. 1. Here the activator is described by a quasi-three-level model: the ground state 0, the intermediate state 1, and the emitting state 2. States 1 and 2 may represent coupled energy levels rather than a single level for specific two-photon UC emissions. As shown, the activator ion at ground state is first excited to state 1 through a phonon-assisted energy transfer from an excited $Yb^{3+}$ ion (ETU1), and further excited to state 2 through a second energy transfer process (ETU2). Subsequently, the UC emission is generated by the transition 2→0.

The power density dependent behavior of the UC emission intensity under continuous wave (CW) excitation can be described by the following steady-state rate equations:

$$\frac{\mathrm{d}N_{\mathrm{Yb1}}}{\mathrm{d}t} = \sigma\rho N_{\mathrm{Yb0}} - \frac{N_{\mathrm{Yb1}}}{\tau_{\mathrm{Yb1}}} = 0, \tag{1a}$$

$$\frac{\mathrm{d}N_1}{\mathrm{d}t} = C_0 N_0 N_{\mathrm{Yb1}} - C_1 N_1 N_{\mathrm{Yb1}} - \frac{N_1}{\tau_1} = 0, \tag{1b}$$

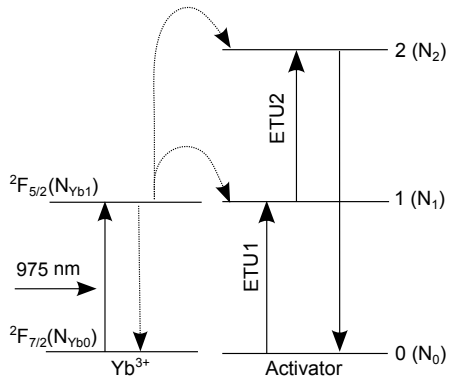


**Fig. 1** Schematic energy level diagrams of the $Yb^{3+}$ and activator ions and the proposed UC mechanism following laser diode excitation at 975 nm. The variables used in the text for the population densities of different levels are indicated within the parentheses.

$$\frac{dN_2}{dt} = C_1 N_1 N_{Yb1} - \frac{N_2}{\tau_2} = 0, \tag{1c}$$

where $\sigma$ is the absorption cross-section of $Yb^{3+}$ ions; $\rho$ is the excitation photon flux, which is linearly related with power density; $\tau_1$ and $\tau_2$ are the lifetimes of activator ions at states 1 and 2, respectively, including both the contributions of radiative and non-radiative relaxation mechanisms, while $\tau_{Yb1}$ is the lifetime of $Yb^{3+}$ ions at $^2F_{5/2}$ state; $C_0$ and $C_1$ are the rate constants for the energy transfer processes ETU1 and ETU2, respectivley. In this model, the depletion of the population of $^2F_{5/2}$ ($Yb^{3+}$) state due to ETU processes is omitted, because the ETU rates at $^2F_{5/2}$ ($Yb^{3+}$) state are much lower than its linear decay rate.[32,33] For the same reason, the contribution to the depletion of state 2 due to ETU to even higher states is not considered either. Under these assumptions, an expression for the population density of state $^2F_{5/2}$ ($Yb^{3+}$) can be obtained

$$N_{Yb1} = \tau_{Yb1}\sigma N_{Yb0}\rho, \tag{2}$$

and the power density dependence of the UC steady-state emission from state 2 can be derived as by rearranging eqns (1a)-(1c)

$$I = \frac{N_2}{\tau_2^{rad}} h\nu = \frac{C_0 C_1 \tau_{Yb1}^2 (\tau_2/\tau_2^{rad}) N_0 h\nu \sigma^2 N_{Yb0}^2 \rho^2}{\frac{1}{\tau_1} + C_1 \tau_{Yb1}\sigma N_{Yb0}\rho}, \tag{3}$$

where $\tau_2^{rad}$ is the radiative lifetime of state 2; $h$ is Planck constant and $\nu$ is the frequency of the UC emission light. The slope efficiency of the UC photoluminescence (PL) intensity with respect to the excitation intensity can be extracted by a linear fit of the data in a double-logarithmic scale, and indicates the multi-photon excitation nature of the UC emission.[27,28] Mathematicaly, this slope efficiency is described by the derivative of log$I$ over log$\rho$, *i.e.*,

$$k \equiv \frac{d\log I}{d\log\rho} = 1 + \frac{1}{1 + \tau_1 \cdot C_1 \tau_{Yb1}\sigma N_{Yb0}\rho}. \tag{4}$$

The details of the derivation of above equation are clarified in section S4 in the electronic supplementary information (ESI). According to eqn (4), the excitation intensity will determine the shape of the power density dependence curve. Under low excitation intensities, where the linear decay rate is dominating over the ETU rate, *i.e.*, $\frac{1}{\tau_1} \gg C_1 \tau_{Yb1}\sigma N_{Yb0}\rho$, the power density dependence curve will appear with a slope of 2.0, indicating a quadratic dependence on the excitation intensity; while under high excitation intensities, where the ETU rate plays a significantly more important role, the curve will appear with a slope of 1.0, *i.e.*, exhibiting a linear dependence on the excitation intensity. In the intermediate range, the slope efficiency changes gradually from 2.0 to 1.0 as the excitation intensity is increased. It is noteworthy to point out that, at the balancing point

$$\rho_b = \frac{1}{\tau_1 \cdot C_1 \tau_{Yb1}\sigma N_{Yb0}}, \tag{5}$$

where the ETU rate and linear decay rate equally contribute to the depopulation of state 1, *i.e.*, $\frac{1}{\tau_1} = C_1 \tau_{Yb1}\sigma N_{Yb0}\rho_b$, the power density dependence curve has a slope efficiency of 1.5.

Based on eqn (3), the QY, $\eta$, of the two-photon UC emission at any power density can be defined by

$$\eta \equiv \frac{I}{\sigma N_{Yb0}\rho h\nu} = \frac{C_0 C_1 \tau_{Yb1}^2 (\tau_2/\tau_2^{rad}) N_0 \sigma N_{Yb0}\rho}{\frac{1}{\tau_1} + C_1 \tau_{Yb1}\sigma N_{Yb0}\rho}. \tag{6}$$

The maximum, $\eta_s$, is reached when the pump power density is at saturation level so that the contribution of the term $\frac{1}{\tau_1}$ can be neglected,

$$\eta_s = C_0 N_0 \tau_{Yb1} \tau_2/\tau_2^{rad}. \tag{7}$$

By inserting eqns (5) and (7) into eqn (6), we obtain

$$\eta = \frac{\eta_s \cdot \frac{\rho}{\rho_b}}{1 + \frac{\rho}{\rho_b}}. \tag{8}$$

Particularly, when the excitation intensity is at the balancing power density, $\rho_b$, the QY is the half of the maximum QY, $\eta_s$, *i.e.*,

$$\eta_b = \eta(\rho = \rho_b) = \frac{\eta_s}{2}. \tag{9}$$

Thus, full QY information can be obtained by determining the balancing power density, $\rho_b$, and corresponding QY, $\eta_b$, because $\rho_b$ characterizes the power density dependence of the QY while twofold $\eta_b$ determines the maximum attainable QY.

The UC mechanisms of most $Yb^{3+}$ sensitized two-photon UC emissions of major activators ($Er^{3+}$, $Ho^{3+}$ and $Tm^{3+}$)

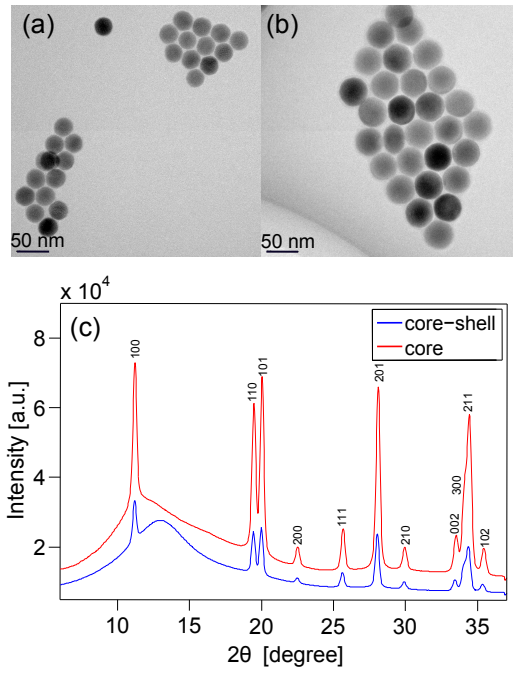


**Fig. 2** TEM images of (a) the core $NaYF_4$:$Yb^{3+}$,$Tm^{3+}$ nanoparticles and (b) the core–shell $NaYF_4$:$Yb^{3+}$,$Tm^{3+}$@$NaYF_4$ nanoparticles. (c) XRD patterns of the synthesized core and core–shell UCNPs.

of UCNPs, including the green emissions of $Er^{3+}$ ions ($^2H_{11/2}/^4S_{3/2}\rightarrow {}^4I_{15/2}$) and $Ho^{3+}$ ions ($^5S_2/^5F_4\rightarrow {}^5I_8$), and the NIR emission of $Tm^{3+}$ ions ($^3H_4\rightarrow{}^3H_6$), have been well determined in the literature.[11,34,35] The simplified model and corresponding conclusions above are valid for all these two-photon UC emissions, as verified by the detailed rate equation analysis based on more reliable and sophisticated models in sections S1–S3 in the ESI. When describing the green UC emission of $Er^{3+}$ ions, the state 2 corresponds to the coupled levels $^4F_{7/2}/^2H_{11/2}/^4S_{3/2}$, achieved by fast non-radiative decay from state $^4F_{7/2}$ to states $^2H_{11/2}/^4S_{3/2}$, while for NIR UC emission of $Tm^{3+}$ ions, the states 1 and 2 correspond to the coupled levels $^3H_5/^3F_4$ and $^3F_{2,3}/^3H_4$, respectively. It is notable that in some special cases the UC emissions mentioned above exhibit cubic power density dependence, *e.g.*, the green UC emission of $Er^{3+}$ ions.[36] In such cases, the proposed approach needs to be modified. In addition, the simplified model does not cover the red UC emissions of $Er^{3+}$ and $Ho^{3+}$ ions, where a more sophisticated model is required due to their slightly different mechanisms.

### 3.2 Morphology, crystalline structure and UC luminescence property of UCNPs

The validity of this approach for QY characterization was tested by investigating the NIR UC emission of two different $Yb^{3+}$/$Tm^{3+}$ codoped samples: core ($NaYF_4$:$Yb^{3+}$,$Tm^{3+}$) and core–shell ($NaYF_4$:$Yb^{3+}$,$Tm^{3+}$@$NaYF_4$) nanoparticles, synthesized through recently reported approaches.[29,30] Figures 2a and 2b show the transmission electron microsope (TEM) images of the synthesized UCNPs. As seen, the core and core–shell nanoparticles appear monodisperse and nearly spherical in shape, and have average diameters of approximate 33 and 43 nm, respectively. The thickness of the shell in core–shell nanoparticles is thus estimated to be 5 nm. The growth of a $NaYF_4$ layer did not change the morphological uniformity. In addition, the phase of the nanoparticles also remained unchanged. Both the core and core–shell nanoparticles have the same phase, verified by the X-ray diffraction (XRD) results shown in Fig. 2c. All the peaks can be well indexed in accordance with the data reported in JCPDS standard card (28-1192), indicating pure hexagonal phase of the nanoparticles.

The PL result of the core nanoparticles under excitation of a CW 975 nm laser diode, shown in Fig. 3, confirms that this NIR UC emission can be treated with the proposed model. As seen, the emission peaks resulting from states $^3F_{2,3}$ and $^3H_5$ at 696 nm ($^3F_{2,3}\rightarrow{}^3H_6$), 1170 nm ($^3F_{2,3}\rightarrow{}^3F_4$), 1650 nm ($^3F_{2,3}\rightarrow{}^3H_5$) and 1220 nm ($^3H_5\rightarrow{}^3H_6$) are absent or significantly weaker compared with those originating from states $^3H_4$ and $^3F_4$ at 800 nm ($^3H_4\rightarrow{}^3H_6$), 1470 nm ($^3H_4\rightarrow{}^3F_4$) and 1850 nm ($^3F_4\rightarrow{}^3H_6$),[37,38] indicating fast non-radiative decays, $^3F_{2,3}\rightsquigarrow{}^3H_4$ and $^3H_5\rightsquigarrow{}^3F_4$.[38,39] The strong emission peak centered at 1035 nm in Fig. 3b originates from the transition of $Yb^{3+}$: $^2F_{5/2}\rightarrow{}^2F_{7/2}$,[40–42] while the emissions in Fig. 3a around 450 nm, 474 nm and 646 nm are generated by the transitions of $Tm^{3+}$: $^1D_2\rightarrow{}^3F_4$, $^1G_4\rightarrow{}^3H_6$ and $^1G_4\rightarrow{}^3F_4$, respectively. The core–shell nanoparticles have very similar PL spectra, thus not shown. It should be noted that the UC emissions in the blue and red spectral regions originating from the states $^1D_2$ and $^1G_4$ are much weaker than the NIR UC emission, even at an excitation power density as high as 125 W/cm$^2$. This supports the treatment of omitting the ETU rate from state 2 to higher energy levels in the theoretical model.

### 3.3 Power density dependence and quantum yield characterization of UCNPs

In order to determine the balancing power density, the power dependence curves for the core and core–shell nanoparticles were measured in a power density span of 0.027–130 W/cm$^2$, as shown in Fig. 4. At the lowest power densities (below 0.05 W/cm$^2$), both the samples appear with a slope of 2.0, indicating two-photon excitation processes. When the excitation power density is increased, the power dependence curves start

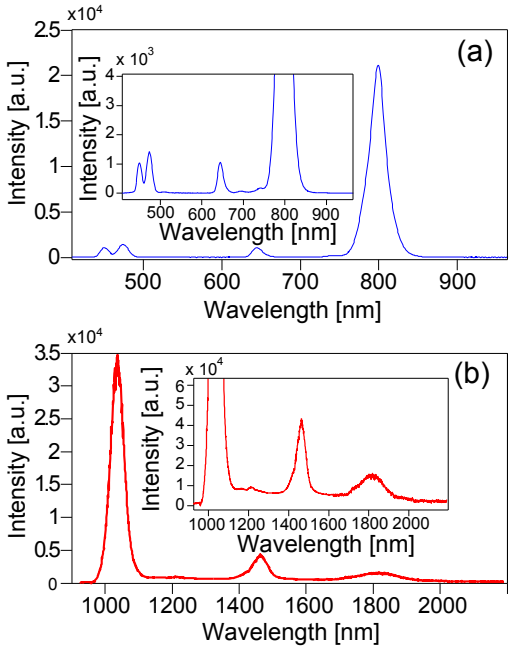


**Fig. 3** (a) The upconversion and (b) the infrared PL spectra of the core $NaYF_4$:$Yb^{3+}$,$Tm^{3+}$ nanoparticles. The insets in Figs. 3a and 3b present the zoomed-in spectra in order to visualize the emission peaks around 700 nm and 1200 nm, respectively. Both spectra were recorded at a power density of 125 W/cm$^2$ under excitation of a CW 975 nm laser diode.

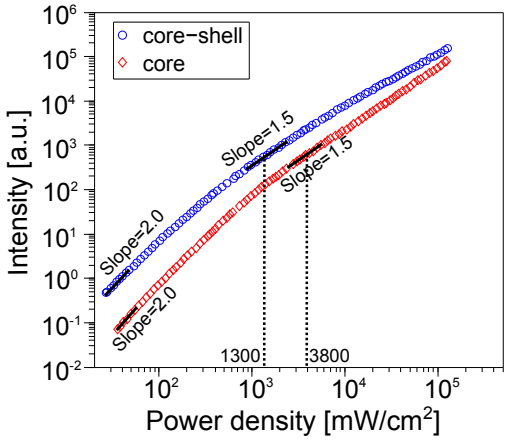


**Fig. 4** The power density dependencies of the NIR UC emission band at 800 nm of the core $NaYF_4$:$Yb^{3+}$,$Tm^{3+}$ nanoparticles (red diamonds) and the core–shell $NaYF_4$:$Yb^{3+}$,$Tm^{3+}$@$NaYF_4$ nanoparticles (blue circles). The black solid lines represent the tangents of the power density dependence curves.

to deviate, with the curve for core–shell nanoparticles deviating earlier than that for core nanoparticles. By fitting the power dependence data with eqn (3) followed by the calculation of the power density giving a slope of 1.5 using eqn (4), the balancing power densities were determined to be approximately 3.8 W/cm$^2$ and 1.3 W/cm$^2$ for the core and core–shell nanoparticles, respectively. As no obvious phase change is found in the XRD patterns of these two samples as shown in Fig. 2c, the smaller value for core–shell nanoparticles could be explained by the longer lifetimes $\tau_1$ and $\tau_{Yb1}$, caused by the protection of the shielding layer epitaxially grown on the core particles.[38,43]

The QYs of the synthesized UCNPs were measured in a power density range of 0.027–20 W/cm$^2$ on a spectrofluorometer-based setup reported in our previous work,[14] as shown in Fig. 5. At the balancing power density, the core and core–shell nanoparticles have QYs of approximately 0.45% and 1.2%, respectively. The fittings of the QY data with eqn (8) were subsequently implemented with the parameter $\rho_b$ locked to the experimentally obtained values. As seen, the QY data can be well fitted both for the core and core–shell nanoparticles, with the fitted maximum attainable QY of 0.91% for the core and 2.6% for core–shell nanoparticles, which can be well estimated by the twofold QY at the balancing power density.

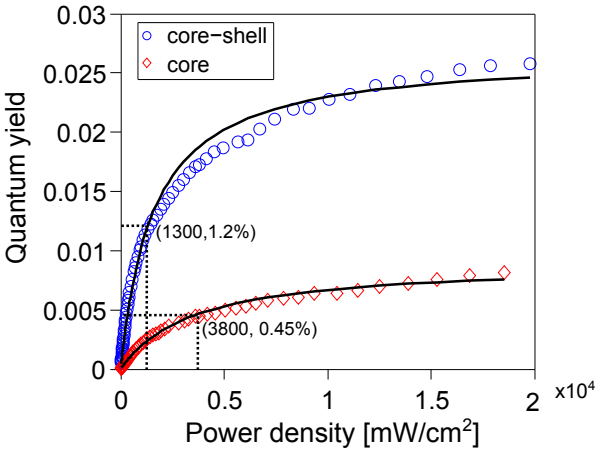


**Fig. 5** The quantum yields of the NIR UC emission band at 800 nm of the core $NaYF_4$:$Yb^{3+}$,$Tm^{3+}$ nanoparticles (red diamonds) and the core–shell $NaYF_4$:$Yb^{3+}$,$Tm^{3+}$@$NaYF_4$ nanoparticles (blue circles) at various excitation power densities. The black solid lines stand for the fitted data.

One main advantage of the proposed approach for QY characterization by providing ($\rho_b$, $2\eta_b$) is that the number of quantitative QY measurements can be dramatically reduced. Especially, measurements under harsh pump conditions (in saturating range) can be avoided, because the balancing power density is significantly lower than the saturation power density. Noticing that the QY starts to decline dramatically when the excitation intensity decreases to below the balancing point ac-

cording to eqn (8), a low balancing power density implies that a considerable QY can be achieved under mild pump conditions. In this sense, the determination of the balancing power density can be used as a fast and simple approach to evaluate the applicability of UCNPs in applications where low excitation intensities are required, such as deep tissue imaging in biological applications. The merit by doing so is that no absolute measurements on luminescence intensities need to be performed, since the balancing power density depends on the trend of the luminescence intensity change instead of absolute intensities.

## 4 Conclusions

To conclude, the QY of $Yb^{3+}$ sensitized two-photon UC emission is theorectically investigated based on a simplified steady-state rate equation model. It is found that the QY can be well characterized by the balancing power density and its corresponding QY. The former describes the power density dependent behavior of the QY, while the latter determines the maximum attainable QY. This is exemplified by experimental measurements on the QYs of core and core–shell $Yb^{3+}/Tm^{3+}$ codoped $NaYF_4$ UCNPs prepared in our lab. Currently, no simple approach exists to characterize the power density dependent QY of UCNPs and thus assess their applicability in biological applications from the perspective of energy conversion. The determination of the balancing power density and its corresponding QY of the proposed method can be used as a fast and simple approach for such purposes.

## Acknowledgments

M. E. Messing and L. R. Wallenberg are gratefully acknowledged for the help with the TEM measurements. J. Larsson is acknowledged for the help with the XRD measurements. D. Hessman is acknowledged for the help with infrared PL measurements. We thank S. Fredriksson, F. Olsson, A. Gisselsson, G. Dumlupinar and X. Wu for the help with the synthesis of the nanoparticles. This work was supported by a grant from the Swedish Research Council (grant No. 621-2011-4265) and a Linneaus grant to the Lund Laser Centre.

## References

1 X. Wang, J. Zhuang, Q. Peng and Y. D. Li, *Nature*, 2005, **437**, 121–124.
2 H.-X. Mai, Y.-W. Zhang, R. Si, Z.-G. Yan, L.-D. Sun, L.-P. You and C.-H. Yan, *J. Am. Chem. Soc.*, 2006, **128**, 6426–6436.
3 J.-C. Boyer, L. A. Cuccia and J. A. Capobianco, *Nano Lett.*, 2007, **7**, 847–852.
4 F. Wang, Y. Han, C. S. Lim, Y. Lu, J. Wang, J. Xu, H. Chen, C. Zhang, M. Hong and X. Liu, *Nature*, 2010, **463**, 1061–1065.
5 F. Wang, R. Deng, J. Wang, Q. Wang, Y. Han, H. Zhu, X. Chen and X. Liu, *Nature Mater.*, 2011, **10**, 968–973.
6 D. K. Chatterjee, A. J. Rufaihah and Y. Zhang, *Biomaterials*, 2008, **29**, 937–943.
7 M. Nyk, R. Kumar, T. Y. Ohulchanskyy, E. J. Bergey and P. N. Prasad, *Nano Lett.*, 2008, **8**, 3834–3838.
8 N. M. Idris, M. K. Gnanasammandhan, J. Zhang, P. C. Ho, R. Mahendran and Y. Zhang, *Nat. Med.*, 2012, **18**, 1580–1585.
9 S. Wu, G. Han, D. J. Milliron, S. Aloni, V. Altoe, D. V. Talapin, B. E. Cohen and P. J. Schuck, *Proc. Natl. Acad. Sci. U.S.A.*, 2009, **106**, 10917–10921.
10 J. Pichaandi, J.-C. Boyer, K. R. Delaney and F. C. J. M. van Veggel, *J. Phys. Chem. C*, 2011, **115**, 19054–19064.
11 F. Auzel, *Chem. Rev.*, 2004, **104**, 139–173.
12 W. Zou, C. Visser, J. A. Maduro, M. S. Pshenichnikov and J. C. Hummelen, *Nature Photon.*, 2012, **6**, 560–564.
13 C. T. Xu, N. Svensson, J. Axelsson, P. Svenmarker, G. Somesfalean, G. Chen, H. Liang, H. Liu, Z. Zhang and S. Andersson-Engels, *Appl. Phys. Lett.*, 2008, **93**, 171103.
14 C. T. Xu, P. Svenmarker, H. Liu, X. Wu, M. E. Messing, L. R. Wallenberg and S. Andersson-Engels, *ACS Nano*, 2012, **6**, 4788–4795.
15 P. Svenmarker, C. T. Xu and S. Andersson-Engels, *Opt. Lett.*, 2010, **35**, 2789–2791.
16 M. Yliharsila, T. Valta, M. Karp, L. Hattara, E. Harju, J. Holsa, P. Saviranta, M. Waris and T. Soukka, *Anal. Chem.*, 2011, **83**, 1456–1461.
17 H. Pakkila, M. Yliharsila, S. Lahtinen, L. Hattara, N. Salminen, R. Arppe, M. Lastusaari, P. Saviranta and T. Soukka, *Anal. Chem.*, 2012, **84**, 8628–8634.
18 C. T. Xu, J. Axelsson and S. Andersson-Engels, *Appl. Phys. Lett.*, 2009, **94**, 251107–251107–3.
19 H. Liu, C. T. Xu and S. Andersson-Engels, *Opt. Lett.*, 2010, **35**, 718–720.
20 J. Zhou, M. Yu, Y. Sun, X. Zhang, X. Zhu, Z. Wu, D. Wu and F. Li, *Biomaterials*, 2011, **32**, 1148 – 1156.
21 C. T. Xu, Q. Zhan, H. Liu, G. Somesfalean, J. Qian, S. He and S. Andersson-Engels, *Laser Photonics Rev.*, 2012, DOI:10.1002/lpor201200052.
22 D. O. Faulkner, S. Petrov, D. D. Perovic, N. P. Kherani and G. A. Ozin, *J. Mater. Chem.*, 2012, **22**, 24330–24334.
23 J.-C. Boyer and F. C. J. M. van Veggel, *Nanoscale*, 2010, **2**, 1417–1419.
24 Q. Liu, Y. Sun, T. Yang, W. Feng, C. Li and F. Li, *J. Am. Chem. Soc.*, 2011, **133**, 17122–17125.
25 A. D. Ostrowski, E. M. Chan, D. J. Gargas, E. M. Katz, G. Han, P. J. Schuck, D. J. Milliron and B. E. Cohen, *ACS Nano*, 2012, **6**, 2686–2692.
26 G. Chen, J. Shen, T. Y. Ohulchanskyy, N. J. Patel, A. Kutikov, Z. Li, J. Song, R. K. Pandey, H. Ågren, P. N. Prasad and G. Han, *ACS Nano*, 2012, **6**, 8280–8287.
27 M. Pollnau, D. R. Gamelin, S. R. Lüthi, H. U. Güdel and M. P. Hehlen, *Phys. Rev. B*, 2000, **61**, 3337–3346.
28 J. F. Suyver, A. Aebischer, S. García-Revilla, P. Gerner and H. U. Güdel, *Phys. Rev. B*, 2005, **71**, 125123.
29 Z. Li and Y. Zhang, *Nanotechnology*, 2008, **19**, 345606.
30 H. Qian and Y. Zhang, *Langmuir*, 2008, **24**, 12123–12125.
31 Y. Cerenius, K. Ståhl, L. A. Svensson, T. Ursby, Å. Oskarsson, J. Albertsson and A. Liljas, *J. Synchrotron Radiat.*, 2000, **7**, 203–208.
32 A. M. Pires, O. A. Serra, S. Heer and H. U. Güdel, *J. Appl. Phys.*, 2005, **98**, 063529.
33 G. Chen, H. Liu, H. Liang, G. Somesfalean and Z. Zhang, *J. Phys. Chem. C*, 2008, **112**, 12030–12036.
34 J. Wright, *Top. Appl. Phys.*, 1976, **15**, 239.
35 G. Chen, H. Liu, G. Somesfalean, H. Liang and Z. Zhang, *Nanotechnology*, 2009, **20**, 385704.
36 F. Song, G. Zhang, M. Shang, H. Tan, J. Yang and F. Meng, *Appl. Phys. Lett.*, 2001, **79**, 1748–1750.
37 T. Schweizer, B. N. Samson, J. R. Hector, W. S. Brocklesby, D. W. Hewak

and D. N. Payne, *J. Opt. Soc. Am. B*, 1999, **16**, 308–316.
38 F. Wang, J. Wang and X. Liu, *Angew. Chem. Int. Ed. Engl.*, 2010, **49**, 7456–7460.
39 G. Chen, T. Y. Ohulchanskyy, R. Kumar, H. Ågren and P. N. Prasad, *ACS Nano*, 2010, **4**, 3163–3168.
40 F. Güell, J. Massons, J. Gavaldà, M. C. Pujol, M. Aguiló and F. Díaz, *J. Appl. Phys.*, 2007, **101**, 033108.
41 L. Huang, S. Shen and A. Jha, *J. Non-Cryst. Solids*, 2004, **345&346**, 349–353.
42 D. Chen, Y. Yu, F. Huang, H. Lin, P. Huang, A. Yang, Z. Wang and Y. Wang, *J. Mater. Chem.*, 2012, **22**, 2632–2640.
43 Y. Wang, K. Liu, X. Liu, K. Dohnalová, T. Gregorkiewicz, X. Kong, M. C. G. Aalders, W. J. Buma and H. Zhang, *J. Phys. Chem. Lett.*, 2011, **2**, 2083–2088.